Journal of Steroid Biochemistry and Molecular Biology 186 (2019) 42–55

Contents lists available at ScienceDirect

Journal of Steroid Biochemistry and Molecular Biology

journal homepage: www.elsevier.com/locate/jsbmb

The intrinsically disordered C-terminal F domain of the ecdysteroid receptor from *Aedes aegypti* exhibits metal ion-binding ability

Anna Więch[a], Magdalena Rowińska-Żyrek[b], Joanna Wątły[b], Aleksandra Czarnota[a], Rafał Hołubowicz[a], Zbigniew Szewczuk[b], Andrzej Ożyhar[a], Marek Orłowski[a,*]

[a] Department of Biochemistry, Faculty of Chemistry, Wrocław University of Science and Technology, 50-370 Wrocław, Poland
[b] Faculty of Chemistry, University of Wrocław, 50-383 Wrocław, Poland

ARTICLE INFO

Keywords:
Aedes aegypti
Ecdysteroid receptor
Zika and dengue vector
nuclear receptors
Intrinsically disordered proteins

ABSTRACT

The dominant vector of dengue and Zika diseases is a female *Aedes aegypti* mosquito. Its reproduction is controlled by the formation of an active heterodimer complex of the 20-hydroxyecdysone receptor (EcR) and Ultraspiracle protein (Usp). Although EcR exhibits a structural and functional organization typical of nuclear receptors (NRs), the EcR C-terminus has an additional F domain (AaFEcR) that is rarely present in the NRs superfamily. The presence of F domains is evolutionarily not well conserved in the NRs. The structure-function relationship of EcR F domains in arthropods is unclear and enigmatic. To date, there have been no data concerning the structure and function of AaFEcR.

Our results showed that AaFEcR belongs to a family of intrinsically disordered proteins (IDPs) and possesses putative pre-molten globule (PMG) characteristics. Unexpectedly, additional amino acid composition *in silico* analyses revealed the presence of short unique repeated Pro-His clusters forming an HGPHPHPHG motif, which is similar to those responsible for Zn^{2+} and Cu^{2+} binding in histidine-proline-rich glycoproteins (HPRGs). Using SEC, SV-AUC and ESI-TOF MS, we showed that the intrinsically disordered AaFEcR is able to bind metal ions and form complexes with these ions. Our studies provide new insight into the structural organization and activities of the F domains of NRs. This unique for the F domains of NRs ion-binding propensity demonstrated by the AaFEcR domain may be a part of the ecdysteroid receptor's mechanism for regulating the expression of genes encoding oxidative stress-protecting proteins.

1. Introduction

Nuclear receptors (NRs) are the ligand-activated transcription factors playing an essential role in modulating the expression of genes involved in development, reproduction, metabolism, stem cell pluripotency and maintaining homeostasis in animals through binding to appropriate DNA response elements [1–5]. Ecdysteroids are the principal arthropod steroid hormones, responsible for reproduction, molting, metamorphosis and development [6–8]. The 20-hydroxyecdysone (20E) hormone acts through a functional receptor formed from the 20E receptor (EcR) [9,10] and Ultraspiracle (Usp), the homologue of the retinoid X receptor (RXR) present in verterbrates [11,12]. *Aedes aegypti* mosquitoes are the main vectors of the world's most devastating human diseases: dengue, chikungunya, Zika and yellow fever [13–16]. Blood is a required nutrient source in order to promote vitellogenesis by these mosquitoes [17,18]. In female hematophagous mosquito species, the blood meal-triggered vitellogenesis is being controlled by 20E and EcR [18,19].

Most NRs share a general structural organization consisting of at least four distinct domains [1]. Structurally, the EcR from *A. aegypti* is similar to other NRs composed of an N-terminal domain (NTD), followed by an evolutionarily conserved DNA-binding domain (DBD), an interdomain linker (hinge), a ligand-binding domain (LBD) and an additional F domain at its C-terminus (Fig. 1.) [10]. The presence of F domains is not conserved in the NR superfamily, and the sequences of F domains are highly variable in both length and sequence. The structure-

Abbreviations: CTD, C-terminal domain; DBD, DNA-binding domain; 20E, 20-hydroxyecdysone; EcR, ecdysteroid receptor; IDPs, intrinsically disordered proteins; IDRs, intrinsically disordered regions; LBD, ligand-binding domain; NTD, N-terminal domain; NRs, nuclear receptors; Usp, product of the *ultraspiracle* gene; Vg, vitellogenin

* Corresponding author at: Department of Biochemistry, Faculty of Chemistry, Wrocław University of Science and Technology, Wybrzeże Wyspiańskiego 27, 50-370 Wrocław, Poland.
E-mail address: marek.orlowski@pwr.edu.pl (M. Orłowski).

https://doi.org/10.1016/j.jsbmb.2018.09.008
Received 25 June 2018; Received in revised form 29 August 2018; Accepted 12 September 2018
Available online 20 September 2018

Fig. 1. Schematic outline of the overall structural organization of AaEcR. AaEcR is composed of NTD (or A/B domain), DBD, the interdomain linker (hinge), LBD and the unique additional F domain (indicated in red) [10]. The lengths of each of the domains in the outline are approximated. Residue numbering corresponds to the sequence of EcR isoform B from *Aedes aegypti* [10] (UniProt ID: P49880/GeneBank: AAA87394.1). Isoform B differs from isoform A (UniProt ID: P49880-1) only in its NTD. (For interpretation of the references to colour in this figure legend, the reader is referred to the web version of this article).

function relationship of the EcR F domains in arthropods is unclear and enigmatic and remains to be explored.

Intrinsically disordered proteins (IDPs), under physiological conditions do not possess a stable and unique three-dimensional (3D) structure and are likely to take part in intermolecular interactions [20]. The lack of a folded rigid structure in IDPs is encoded in their amino acid sequence. Interestingly, for some IDPs, the phenomenon of metal ion binding occurs either as part of their function or in the pathogenesis of diseases. In particular, in the case of Starmaker (Stm) protein, Ca^{2+} binding is important in biomineralization [21], whereas in Alzheimer's disease, Zn^{2+} or Cu^{2+} binding by β-amyloids causes the creation of metal-enriched amyloid plaques [22].

The current knowledge about the role the F domain plays in NR functions is rather residual. It was suggested that the residual F domains of mammalian NRs might be involved in the receptor activity by affecting transcriptional activation, the stabilization of ligand binding by LBDs and dimerization [23].

Importantly, the presence of F domains is not well conserved evolutionarily in all members of the NR superfamily. In the present study, we characterized the biophysical and biochemical properties of the isolated F domain of the EcR from *A. aegypti* (AaFEcR). The extensive experimental data, supported by *in silico* analyses, indicate that AaFEcR exhibits the common characteristics of IDRs and IDPs possessing a putative pre-molten globule (PMG) shape. Importantly, we found that AaFEcR exhibits metal ion-binding ability by forming diverse complexes with Zn^{2+}, Cu^{2+} and Ca^{2+} ions. Thus, another important region of NRs, apart from the DBD, is able to specifically bind metal ions. Our studies provide new insight into the structural organization and activities of the F domains of NRs. The ion-binding propensity demonstrated by AaFEcR may be a physiologically significant part of the EcR regulatory mechanism. The importance of these findings is discussed.

2. Materials and methods

2.1. Buffer composition

Buffer L (lysis buffer; 50 mM Na_2HPO_4 (ROTH), 150 mM NaCl (Merck), and 1 mM dithiothreitol (DTT, Sigma-Aldrich), pH 7.5); buffer A (fusion protein wash buffer; 50 mM Na_2HPO_4, 600 mM NaCl, 10% glycerol (ROTH), and 1 mM β-mercaptoethanol (ROTH), pH 7.5); buffer B (fusion protein elution buffer; 50 mM Na_2HPO_4, 150 mM NaCl, 250 mM imidazole (Merck), 10% glycerol, and 1 mM β-mercaptoethanol, pH 7.5); buffer C (fusion protein gel filtration buffer; 50 mM Na_2HPO_4, 150 mM NaCl, 10% glycerol, and 1 mM β-mercaptoethanol, pH 7.5); buffer D (gel filtration buffer; 10 mM Tris-HCl (ROTH) and 150 mM NaCl, pH 7.0); buffer E (10 mM Tris-HCl, 150 mM NaCl, and 1 mM $ZnCl_2$ (Sigma-Aldrich), pH 7.0); buffer F (10 mM Tris-HCl, 150 mM NaCl, and 0.5 mM $CuCl_2$ (ROTH), pH 7.0); buffer G (10 mM Tris-HCl, 150 mM NaCl, and 1 mM $CaCl_2$ (Merck), pH 7.0).

2.2. DNA construct

The plasmid pAc5-Aa-EcR-B with cDNA encoding the full-length EcR isoform B from *Aedes aegypti* [24] (UniProt ID: P49880/GeneBank: AAA87394.1), kindly provided by Professor Alexander Raikhel (Department of Entomology, Institute for Integrative Genome Biology, Center for Disease Vector Research), was used as the template for PCR. The cDNA encoding the F domain of the EcR from the *Aedes aegypti* (AaFEcR) sequence from amino acid residue 564 (L564) was amplified using the forward primer (5′-gccgcc*CATATG*CTGGAGGAGATCTGGGACGTC-3′) and the reverse primer (5′-gccgcg*GTCGAC*CTATACCTGGTCGAGCATGCCGAG-3′) in a pCold™TF DNA vector (Takara/Clontech). The plasmid is a cold inducible vector that allows the trigger factor (TF) chaperonin to fuse to the N-terminus of a protein of interest, increasing its quantity and solubility. The forward primer sequence introduced the restriction site for *Nde*I, and the reverse primer sequence introduced the restriction site for *Sal*I. The introduced restrictions sites are marked in italics. The introduced sequence corresponding to the STOP codon is underlined. The uppercase letters in the primer sequences denote a sequence derived from the cDNA of the EcR, while the lowercase letters represent nucleotides added for cloning purposes. The correctness of the performed cloning was confirmed by DNA sequencing.

2.3. Protein expression and purification

The recombinant fusion protein TF-AaFEcR was expressed in the *E. coli* BL21(DE3)pLysS strain (Novagen). Overexpression of AaFEcR fused with TF in the pCold™ TF DNA vector provided the stable, full-length product. Our previous attempts to overexpress AaFEcR in many other vectors were not satisfactory because the protein tended to degrade during overexpression (data not shown). The cells were grown in 0.5 l of Terrific Broth medium (TB; Invitrogen) supplemented with 100 μg/ml carbenicillin (ROTH) and 35 μg/ml chloramphenicol (Calbiochem) at 37 °C. When OD_{600} of the culture reached 0.5, the culture was cooled at 16 °C for 30 min. Subsequently, expression of the protein was induced by isopropyl-β-D-thiogalactopyranoside (IPTG, ROTH) at a final concentration of 0.25 mM. After 12 h of incubation, the culture was centrifuged (4500 × *g*, 4 °C, 25 min), and the obtained cell pellet was washed in buffer L (10 ml of buffer for every 1 g of cell pellet). Subsequently, the washed cell pellet was centrifuged (4000 × *g*, 4 °C, 12 min), and the cell pellet was resuspended again and frozen at −80 °C. The cells were lysed by quick thawing in a water bath at 25 °C. Immediately, the cell lysate was supplemented with PMSF (final concentration of 0.4 mg/ml; Sigma-Aldrich), DNAse I (10 μg/ml, Sigma-Aldrich) and RNase A (15 μg/ml, Sigma-Aldrich). The suspension was incubated at 4 °C until its viscosity decreased and then centrifuged (17,500 × *g*, 4 °C, 45 min). The supernatant was subsequently supplemented with PMSF again (0.4 mg/ml) and incubated for 1 h at 4 °C with 1 ml of TALON™ Metal Affinity Resin (Clontech) equilibrated with buffer L. The incubation time of TF-AaFEcR with TALON™ Metal Affinity Resin was optimized to 60 min. No significant differences in the obtained amount of TF-AaFEcR were observed with a longer incubation time. After the incubation, a gravity flow column (20 ml) was packed with the resin. The resin was then washed with 20 ml of buffer A and packed into a 5/50 Tricorn™ column (GE Healthcare). The column was subsequently attached to an ÄKTAexplorer system (GE Healthcare). The resin was washed first with buffer A until the value of A_{280} was stable in order to remove proteins that bound to TALON™ Metal Affinity Resin nonspecifically and then with buffer C until the conductivity stabilized. TF-AaFEcR was eluted with buffer B at a flow rate of 0.25 ml/min. Collected fractions were pooled and concentrated to 0.25 ml using the Amicon Ultra-4 Centrifugal Filter Unit (Merck/Millipore; molecular weight cut-off (MWCO) 30.0 kDa). To obtain homogeneous TF-AaFEcR, the sample was further purified by gel filtration on a Superdex 75 10/300 G L (GE Healthcare) column in buffer C at 0.5 ml/min. The elution of the fusion protein was monitored at 280 nm. The purity of the

samples was analyzed by SDS-PAGE. After the gel filtration, the obtained amount of TF-AaFEcR was no less than 10 mg from 0.5 L of the bacterial culture. Fractions containing purified TF-AaFEcR were pooled, concentrated to 500 µl and digested with 2.5 U of HRV3C protease (Sino Biological Inc.) per 1 mg of fusion protein for 18 h at room temperature. Subsequently, the mixture of TF-free AaFEcR, TF and HRV3C protease was subjected to gel filtration chromatography on a Superdex 75 10/300 G L column equilibrated with buffer D or L. The gel filtration was performed at flow rate 0.5 ml/min on the ÄKTAexplorer system. The elution profile was monitored at 280 nm, and fractions of 0.5 ml were collected. After cleavage and gel filtration, the obtained amount of AaFEcR was reproducible and was no less than 2 mg from 0.5 L of the bacterial culture. The samples showed the homogeneity in terms of quality and purity, and appropriate experiments were conducted using AaFEcR from different preparations. SDS-PAGE analysis of samples from different stages of AaFEcR purification is presented in Suppl. Fig. 1. The identity of the recombinant AaFEcR was confirmed by Western blot analyses using anti-His monoclonal mouse antibodies (data not shown). The molecular mass of AaFEcR was confirmed by ESI-TOF mass spectrometry. The molecular mass calculated for the minor peak (13,294.09 Da) was confirmed by the theoretical mass estimated with the ProtParam tool (https://web.expasy.org/protparam/).

2.4. SDS-PAGE analysis

All protein samples obtained during the purification procedure were analyzed according to [25]. Protein samples were boiled for 10 min at 95 °C in SDS sample buffer containing β-mercaptoethanol and then centrifuged at 20,000 × *g* at room temperature for 10 min. Proteins were separated using 12% gels with a constant current of 20 mA for 1 gel. After electrophoresis, the gels were stained with Coomassie Brilliant Blue R-250 [26] and analyzed using Image Lab™ Software (Bio-Rad).

2.5. Determination of the molecular weight of AaFEcR and the formed Zn^{2+}-, Cu^{2+}- or Ca^{2+}-AaFEcR complexes with ESI-TOF mass spectrometry

A volume corresponding to 100 ng of AaFEcR was injected into a PepRPC HR 5/5 column (GE Healthcare) in order to perform reversed-phase liquid chromatography. The mobile phase at a flow rate of 1 ml/min was composed of solvent A (0.05% trifluoroacetic acid (TFA), Fluka) in H_2O) and solvent B (0.04% TFA in 70% acetonitrile (Fluka)). The protein was eluted using a linear gradient of buffer B (0–100%) for 30 min, and each fraction of 0.3 ml was collected. A microOTOF-Q2 spectrometer (Bruker Daltonics) calibrated with ESI-TOF Tuning Mix (Sigma-Aldrich) with the Apollo II2 ion funnel electrospray ionization source was used to record the mass spectrum in the range 600–2000 m/z. The AaFEcR sample was released at a flow rate of 3 µl/min at 200 °C. Data analysis was performed with the DataAnalysis™program (Bruker Daltonics). High-resolution mass spectra for AaFEcR complexes with metal ions were obtained on a Bruker micrOTOF-Q spectrometer (Bruker Daltonik, Bremen, Germany) equipped with an Apollo II electrospray ionization source with an ion funnel. The mass spectrometer was operated in the positive ion mode. The instrumental parameters were as follows: scan range *m/z* 300–4000, dry gas–nitrogen, temperature 170 °C, ion energy 5 eV. The capillary voltage was optimized to the highest S/N ratio and was 4500 V. The small changes in voltage (± 500 V) did not significantly affect the optimized spectra. The samples (metal:AaFEcR in 1:1 and 1:2 stoichiometries, $[AaFEcR]_{tot} = 10^{-5}$ M) were prepared in a 1:1 acetonitrile-water mixture at pH 7.2. Zn(II), Cu(II) and Ca(II) perchlorate salts were used (Sigma-Aldrich). Variations in the solvent composition down to 5% acetonitrile did not change the species composition. The sample was infused at a flow rate of 3 µl/min. The instrument was calibrated externally with the Tunemix™ mixture (Bruker Daltonics, Germany) in quadratic regression mode. Data were processed by using the Bruker Compass Data Analysis 4.2 program. The mass accuracy for the calibration was better than 5 ppm; along with the true isotopic pattern (using SigmaFit (Bruker Daltonics)), this accuracy enabled an unambiguous confirmation of the elemental composition of the obtained complex.

2.6. In silico analysis

All *in silico* analyses were conducted similarly to those described in [27]. The structural disorder within AaFEcR was analyzed using predictors such as IUPred at http://iupred.enzim.hu/ [28], PONDR VLXT at http://www.pondr.com/ [29–31], PONDR-FIT at http://www.disprot.org/pondr-fit.php [32] and DISOPRED at http://bioinf.cs.ucl.ac.uk/introduction/ [33]. The amino acid composition of AaFEcR was analyzed by Composition Profiler at http://www.cprofiler.org/ [34]. The analysis of the distribution of disordered and ordered regions in AaFEcR was made by FoldIndex© at http://bip.weizmann.ac.il/fldbin/findex/ [35]. Presence of a disordered region in AaFEcR is considered to occur with a FoldIndex value below 0.0. The charge *versus* hydropathy plot was created using the algorithm available at http://www.pondr.com/ [29,36].

2.7. Analytical size exclusion chromatography

The initial procedure for size exclusion chromatography (SEC) was similar to the protocol described recently [27]. SEC was performed using Superdex 75 10/300 G L and the ÄKTAexplorer system. The column was equilibrated initially with buffer D, and the chromatography was performed at a flow rate of 0.5 ml/min at room temperature. The elution profile was monitored at 280 nm. To establish the gel phase distribution coefficient (K_{av}), the calibration of the column was carried out. Samples of standard proteins samples (0.25 ml with a concentration of 0.15 mg/ml): bovine serum albumin (3.55 nm), ovalbumin (3.05 nm), chymotrypsinogen (2.09 nm), RNase A (1.75 nm) and cytochrome C (1.70 nm) and 0.25 ml samples of AaFEcR with concentrations of 0.5, 1.0 and 2.0 mg/ml were injected into the column. The elution volume of every sample (V_e) was used to calculate K_{av} according to the equation: $K_{av} = (V_e - V_0)/(V_c - V_0)$ [37]. The column void volume (V_0) was established by blue dextran with a value equal to 8.39 ml, and the column volume (V_c) was 24 ml. The K_{av} values of standard proteins were subsequently plotted against their Stokes radius (R_S) values and fitted to a standard curve. The elution peaks for 0.5 mg/ml, 1.0 mg/ml and 2.0 mg/ml correspond to the following K_{av} values: 0.202, 0.198, and 0.196, respectively. The R_S value of AaFEcR was calculated according to obtained standard curve equation. SEC of AaFEcR in the presence of guanidinium chloride (GdmCl, Sigma) was carried using Superdex 75 10/300 G L. Samples of 0.2 ml with a protein concentration of 0.5 mg/ml were incubated with the appropriate amount of GdmCl for 1 h at room temperature. The column was equilibrated with buffer D containing the appropriate concentration of GdmCl. After the incubation, the samples were loaded onto the column. The obtained elution volumes enabled calculation of K_{av} and R_S in the same way as described above. SEC experiments in the presence of metal ions were carried out on the Superdex 75 10/300 G L. The column was equilibrated with buffer D with the appropriate amount of buffer E (for SEC in the presence of Zn^{2+}), buffer F (for SEC in the presence of Cu^{2+}) or buffer G (for SEC in the presence of Ca^{2+}). Samples of 0.25 ml of AaFEcR at a concentration of 0.5 mg/ml were incubated with the appropriate amount of metal ion at room temperature for 1 h and then loaded onto the column. The elution volume of every sample was subsequently used to calculate each K_{av} and R_S as described above.

2.8. Circular dichroism spectroscopy

All CD spectra were recorded using a JASCO J-715 CD-spectropolarimeter (Japan) at 20 °C. The Peltier Type Temperature Control System (JASCO, Japan) was responsible for maintaining a constant

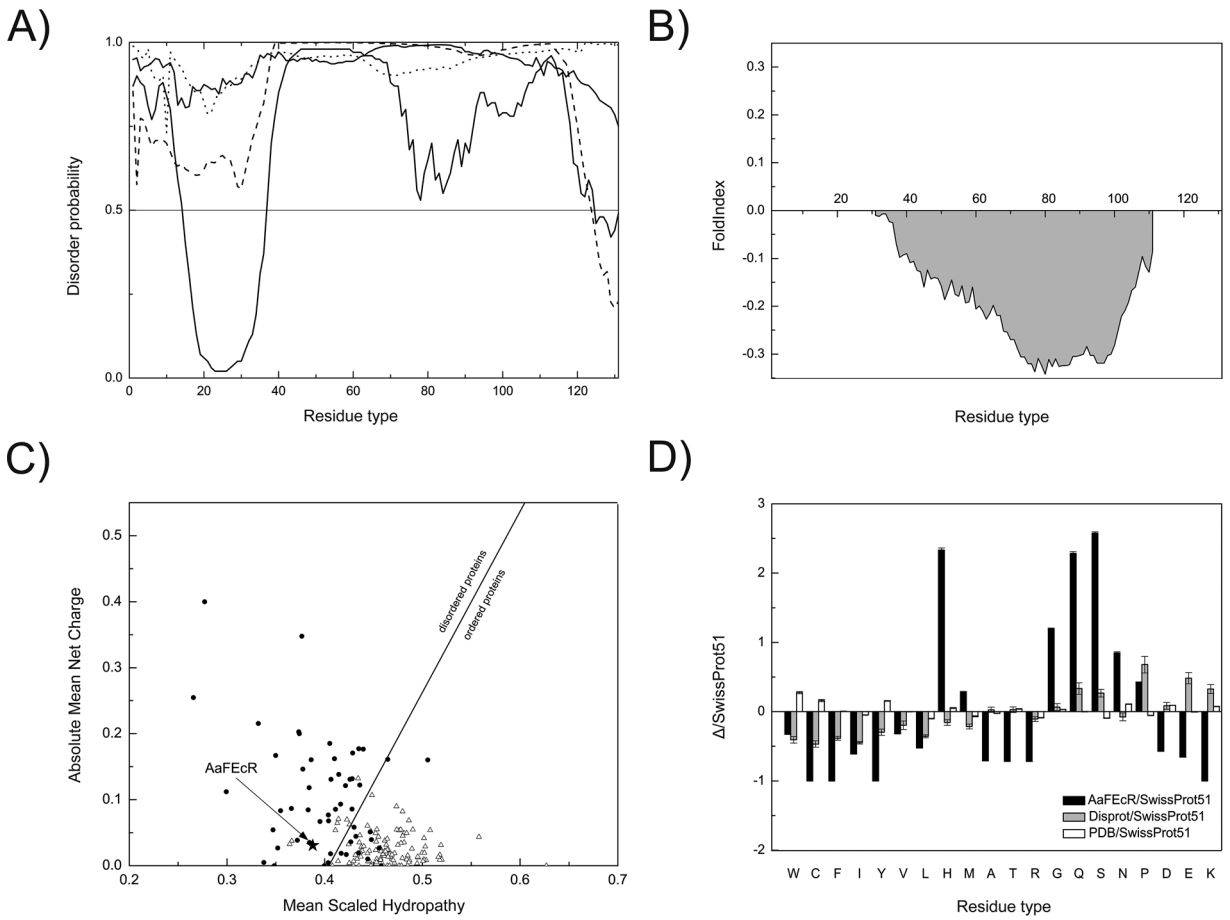

Fig. 2. *In silico* analyses of AaFEcR amino acid sequence indicate disorder occurrence. A) Structural disorder probability predicted for AaFEcR with the IUPred (bold, solid line), PONDR VLXT (dashed line), PONDR-FIT (dotted line) and DISOPRED (solid line) algorithms. B) Potential disorder occurrence in AaFEcR was marked with grey area. C) Absolute mean net charge plotted against mean scaled hydropathy for disordered proteins (black dots) and ordered proteins (triangles) [29,36]. AaFEcR, marked with an asterisk, belongs to the group of disordered proteins. D) AaFEcR amino acid composition analysis performed with Composition Profiler. Amino acid residues were ranked on the basis of side chain stiffness for from the rigid residues to the most flexible residues.

temperature of 20 °C in the cell. Data were collected in triplicate at a scanning speed of 20 nm/min. Using a 1 mm path length cell, far-UV spectra of native AaFEcR were recorded from 260 to 197 nm. For every sample, a corresponding baseline with buffer solutions in which the protein was incubated (for structure-inducing and unfolding experiments - buffer L (without DTT) and derivatives containing trifluoroethanol (TFE, Sigma-Aldrich) or GdmCl, respectively; for protein-metal ion interactions - buffer D and derivatives containing the appropriate amount of buffers E, F or G) were recorded. Every sample contained AaFEcR at a concentration equal to 10 μM. A corresponding average baseline spectrum was subtracted from the average sample spectrum. All collected spectra were smoothed with a Savitzky-Golay filter [38] and subsequently converted to molar residual ellipticity units according to [39]. CDPro software (CDSSTR and CONTIN/LL algorithms) and IBasis 7 [40] were used to estimate the secondary structure composition of AaFEcR. To conduct structure-inducing experiments, AaFEcR was incubated with the appropriate concentration of TFE for 30 min at room temperature before CD spectra were recorded. For the 10% concentration of TFE, spectra were recorded from 260 to 196 nm, while samples with other concentrations of TFE were recorded from 260 to 195 nm. The unfolding experiment was conducted as follows: AaFEcR was incubated for 1 h in the presence of the appropriate concentration of GdmCl before CD spectra were recorded. All spectra in the presence of GdmCl were recorded from 260 to 202 nm, 205 nm, 206 nm, 210 nm, 209 nm, and 212 nm for 0.1 M, 0.3 M, 0.5 M, 1 M, 3 M and 6 M concentrations of GdmCl, respectively. The spectra are terminated at the wavelength where the voltage value is lower than 600 mV. Therefore, it is impossible to observe the standard decrease in molar residual ellipticity at ~200 nm (θ_{200}) with increasing concentration of denaturant (GdmCl) [41]. Spectra concerning metal ions that would influence the secondary structure composition of AaFEcR were recorded from 260 to 195 nm. The other parameters remained as described above. AaFEcR was incubated for 30 min at room temperature with a proper amount of buffer E (for CD in the presence of Zn^{2+}), F (for CD in the presence of Cu^{2+}) or G (for CD in the presence of Ca^{2+}).

2.9. Analytical ultracentrifugation experiments

The sedimentation velocity (SV) analytical ultracentrifugation experiment was conducted in a Beckman Coulter ProteomeLab XL-I ultracentrifuge (Software version 6.0, Beckman Coulter Inc., Brea, CA, USA). An An-60Ti rotor and cells with charcoal-filled Epon® centerpieces and sapphire windows were used. The sample sector contained 400 μl of AaFEcR in buffer D, whereas the reference sector contained only 400 μl of buffer D. The experiment was conducted overnight at 50,000 rpm and 20 °C. Sedimentation was monitored by laser interferometry and absorbance at 280 nm. Both sets of results were highly consistent; therefore, only the analysis of interferometric data is presented. Time-corrected data [42] were analyzed using SEDFIT software (http://www.analyticalultracentrifugation.com). The density (1.005 g/ml) and dynamic viscosity of a buffer (1.018 cP), as well as the partial specific volume of AaFEcR (0.689 ml/g) at 20 °C, were calculated using SEDNTERP (http://sednterp.unh.edu/). The sedimentation coefficient (s), frictional ratio (f/f_0) and apparent

molecular weight (MW_{app}) were calculated using the continuous $c(s)$ distribution model with at least 10 points per 1 S. Maximum entropy regularization with $p = 0.68$ was applied [43]. The quality of the fits was assessed using root mean square deviation (RMSD) values and residual distributions.

3. Results

3.1. In silico prediction of the intrinsically disordered content in AaFEcR

The presence and extent of IDRs in AaFEcR were predicted using IUPred [28] and PONDR-FIT [32]. The results obtained with these algorithms indicated that the whole structure of AaFEcR should be disordered (Fig. 2A). The results obtained from PONDR VLXT [30] indicated the presence of a disordered region between amino acids 1 and 123 (Fig. 2A). In contrast, the DISOPRED algorithm [33] indicated the occurrence of ordered regions between amino acids 16 and 36 and from amino acids 125 to 131 (Fig. 2A). Additional *in silico* analysis using FoldIndex revealed that the region between amino acids 31 and 114 in AaFEcR may be classified as disordered (Fig. 2B). IDPs are likely to possess an unusual amino acid composition, because the protein structure disorder is driven by a high net charge and a low mean hydrophobicity [44]. For further verification of the hypothesis concerning AaFEcR as an IDP, we also used a charge-hydropathy plot. The mean scaled hydropathy and absolute mean net charge were calculated [44] for isolated AaFEcR, and above values placed AaFEcR among the IDPs (Fig. 2C). In Fig. 2D, the amino acid composition analysis of AaFEcR indicates considerable ($\Delta \sim 1$) enrichment of the H, G, Q, S, and N amino acids and depletion of the C, F, Y, and K amino acids compared to the average content in the Swiss-Prot database. Similar tendencies for a change in amino acid content were observed by comparing the information in the DisProt and Swiss-Prot databases, and the result is consistent with the disorder predictions for AaFEcR. In conclusion, amino acid sequence *in silico* analyses clearly demonstrated that this domain may belong to a family of IDRs.

3.2. AaFEcR exhibits characteristics of IDPs

Far-UV circular dichorism (CD) spectroscopy was used to determine the secondary structure content in AaFEcR. Typical for IDPs features were observed for the native spectrum (Fig. 3A), such as: the presence of a minimum at ~200 nm and the lack of a distinct minima at 208 nm and 222 nm [45]. The unfolding of residual secondary structures in AaFEcR was examined with far-UV CD in the presence of GdmCl (Fig. 3A). Increasing the concentration of GdmCl enabled us to observe an increase in the molar residual ellipticity value at ~222 nm (θ_{222}) values. Up to the 0.5 M GdmCl concentration, there were no significant changes in the θ_{222} values for samples containing native AaFEcR and AaFEcR with denaturant. However, for higher (1 M, 3 M and 6 M) concentrations of GdmCl, we observed an increase in the θ_{222} value, indicating the loss of the residual ordered secondary structures. The structure-forming potential of AaFEcR was investigated by recording the spectra of AaFEcR with trifluoroethanol (TFE) (Fig. 3B). The spectrum recorded in 10% TFE possesses almost the same shape as the native spectrum. The spectrum of AaFEcR in 20% TFE was an intermediate between the features typical of IDPs and globular proteins. Two negative minima at 203 nm and 224 nm occurred, indicating an increase in the ordered secondary structure content of AaFEcR. The spectra of samples with 40%, 60% and 80% TFE have a similar shape but different values of θ at ~208 nm and ~222 nm. The shape of the two spectra recorded in the presence of 60% and 80% TFE is almost identical; thus, in the presence of 60% TFE, AaFEcR can be considered fully structured. The deconvolution of the native AaFEcR spectrum presented in Fig. 3C reveals that the amount of unordered regions was 55.45% ± 13.08%. With AaFEcR having approximately 30% ordered secondary structures, it is interesting how little GdmCl at concentrations up to 3 M influenced the secondary structure content (Fig. 3A). Two subclasses of IDPs are known: coil-like (with no significant secondary structure content) and PMG-like (more compact with residual secondary structure) [44]. The results obtained for AaFEcR, compared with data for coil-like and PMG-like IDPs, placed AaFEcR among PMG-like IDPs (Fig. 3D). Such IDPs are characterized by the lack of a stiff 3D structure, even in the presence of ~50% secondary structure content. This analysis is compatible with the deconvolution results depicted for AaFEcR in Fig. 3C.

3.3. Hydrodynamic properties of AaFEcR

Sedimentation velocity analytical ultracentrifugation (SV-AUC) and a series of size exclusion chromatography (SEC) were conducted in order to determine hydrodynamic properties of AaFEcR. The value of the Stokes radius (R_S) for the native AaFEcR is 2.67 nm ± 0.1 nm (Figs. 4A and 5). Using equations derived from [46], theoretical values of R_S for AaFEcR considered as a native globular protein, a natively unfolded (NU) coil and a NU-PMG were calculated, plotted together with the value obtained experimentally and presented in Fig. 5. The most similar to determined by SEC R_S value was the one calculated for NU-PMG, what confirms the results obtained from CD spectroscopy analysis (Fig. 3D). Transforming the standard curve equation enabled us to determine the theoretical mass of a molecule with an R_S value of 2.67 nm (M_{theor} = 38,800 g/mol). The ratio of M_{theor}/M_{exp} equals 2.918, and the presence of only one elution peak initially suggested that AaFEcR might exist as a trimer. However, further experiments, such as SEC in the presence of GdmCl and SV-AUC, refute this supposition. The SEC experiment for AaFEcR was conducted in the presence of GdmCl, and the change in AaFEcR R_S is presented in Fig. 4B. For every sample, only one elution peak was observed (data not shown), indicating that dissociation of the protein subunits does not occur. Notably, the standard deviation tended to decrease with increasing GdmCl concentration (up to 2 M). This finding indicates that at lower denaturant concentrations, AaFEcR molecules remain dynamic and can change their conformation. The SV-AUC experiment was conducted to verify whether the high R_S of AaFEcR observed in SEC experiments is a result of oligomerization or possibly of structural disorder. The results are summarized in Fig. 4C and Table 1. The sedimentation coefficient distributions (Fig. 4C) calculated from the SV-AUC data indicate that one major species with a sedimentation coefficient of approximately 1.2 S and a hydrodynamic radius (R_h) slightly greater than 2.9 nm is present in all samples of AaFEcR at different concentrations ranging from 0.15 mg/ml to 1.0 mg/ml range (Table 1). The R_h value calculated from the SV data is higher than that R_s calculated from the SEC elution profiles. This finding was observed in our laboratory previously for highly anionic IDPs and may be caused by nonideal sedimentation of the protein or co-sedimentation with bound counterions [47]. No significant dependence of the sedimentation coefficient on the protein concentration was observed (Table 1), as the c(s) distributions obtained for different protein concentrations nearly overlapped (data not shown). The frictional ratio (f/f_0) of 1.9–2.0, higher than the approximate value of 1.3 expected for a typical globular protein such as bovine serum albumin (BSA), indicates that the protein has an extended conformation. The relation between the frictional ratio and the molecular weight of a protein is an indicative of protein disorder [48]. Fitting the apparent molecular weight (MW_{app}) of AaFEcR calculated using the SV data for all three tested concentrations indicated existence of AaFEcR as a monomer.

3.4. AaFEcR is able to bind metal ions

Additional *in silico* sequence analysis of AaFEcR indicated the presence of a specific amino acid motif, HGPHPHPHG (residues 617 to 625), resembling the one present in histidine-proline-rich glycoproteins (HPRGs) (Fig. 6.) [49], which is responsible for Zn^{2+} and Cu^{2+} binding

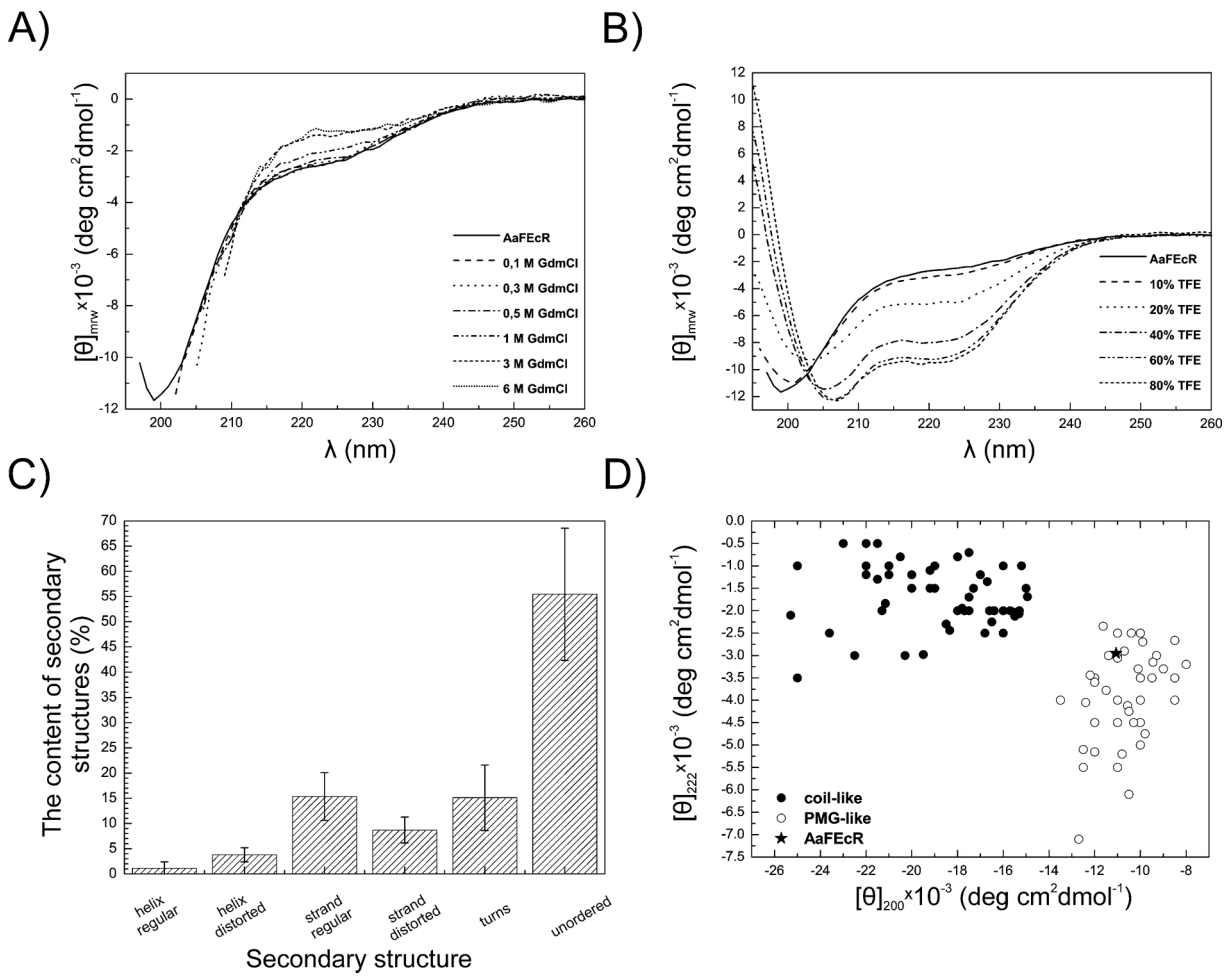

Fig. 3. Intrinsically disordered AaFEcR possesses residual secondary structures. A) Far-UV CD spectra of AaFEcR in the presence of different GdmCl concentrations (samples containing GdmCl are marked with dashed and dotted lines). B) Far-UV CD spectra of AaFEcR (solid line) recorded in the presence of different TFE concentration (marked with dashed or dotted lines). C) Deconvolution of the far-UV spectrum for native AaFEcR. D) Double wavelength plot [44] positioning AaFEcR (asterisk) among proteins conforming to a PMG-like shape (empty circle) instead of among coil-like proteins (black dots). Experiments presented in A) and B) were performed in triplicate and the obtained results were averaged.

(see 4. Discussion). To investigate in detail whether AaFEcR is capable of binding Zn^{2+} and Cu^{2+} and whether this interaction is exclusive to d-block metal ions (parallel experiments using Ca^{2+} were conducted to examine the exclusivity), we first investigated the influence of ions on the hydrodynamic properties of AaFEcR (Fig. 4D). Injected samples were prepared to determine the specific molar ratio between metal ions and AaFEcR (nM^{2+}/nAaFEcR). For all samples with nM^{2+}/nAaFEcR equal to 0.05, the AaFEcR R_S slightly increased. A difference in the ion-AaFEcR interaction was observed for samples with higher metal ion/protein ratios. For the samples of AaFEcR containing Ca^{2+} (up to a 2.5-fold excess) the overall range of observed changes in the R_S values was much smaller than in the presence of Zn^{2+} or Cu^{2+}. Namely, in up to a 2.5-fold excess of Ca^{2+} ions, the hydrodynamic volume of AaFEcR molecules became only slightly greater than the hydrodynamic volume determined for the native protein. It is probably related to only a small change in the shape of the domain caused by interaction with Ca^{2+}. In contrast to this, the R_S of AaFEcR in the presence of 2.5-fold excess of Zn^{2+} and Cu^{2+} clearly decreased from the 2.67 nm ± 0.1 nm to 2.44 nm ± 0.04 nm and 2.47 nm ± 0.02 nm, respectively. When the metal ion excess was greater than 2.5-fold, the R_S of AaFEcR did not change (data not shown), indicating metal ion saturation of the protein molecule. The effect of the presence of metal ions on the possible secondary structure formation in AaFEcR was examined with CD spectroscopy. The obtained CD spectra for samples containing AaFEcR with the appropriate metal ion concentration (data not shown) did not indicate significant secondary structure formation. In the presence of increasing concentration of Zn^{2+}, with AaFEcR:Zn^{2+} molar ratios of 1 and 2.5, the θ_{200} value slightly increased, but the θ_{222} value remained unchanged. The opposite tendency was observed for samples with Cu^{2+}, where the θ_{200} value was stable and the θ_{222} values slightly decreased for all samples. The CD spectra for AaFEcR in the presence of Ca^{2+} overlapped with each other (data not shown). Further deconvolution of the obtained data did not indicate any statistically relevant changes in the secondary structure content of AaFEcR. Therefore, we suggest that the AaFEcR interactions with Zn^{2+} and Cu^{2+} do not generate significant secondary structure but result in protein compaction.

Electrospray mass spectrometry (ESI-TOF MS) confirmed the findings discussed above and showed the stoichiometry of metal-AaFEcR complexes. Calculated, experimental *m/z* values and their isotopic patterns were compared enabling precise peak assignments. Species with z = 8+ to 20+ were observed. In the case of all three metal species, 1:1 complexes dominate in solutions with a 1:1 metal-to-ligand ratio (Figs. 7–9).

Mononuclear zinc complexes are visible at *m/z* = 1336.8 $[ZnAaFEcR]^{10+}$ and 1340.5 $[ZnAaFEcRK]^{10+}$. These metal complex signals prevailed when a 1:1 metal-to-ligand ratio was used, although a minor signal at *m/z* = 1346.9 corresponding to a bimetallic complex $[Zn_2AaFEcRK]^{10+}$ was also observed (Fig. 7). When an excess amount of Zn(II) was added (Zn(II) to metal ratio = 2:1), the intensity of the signals at *m/z* = 1336.8 $[ZnAaFEcR]^{10+}$, 1340.5 $[ZnAaFEcRK]^{10+}$ and

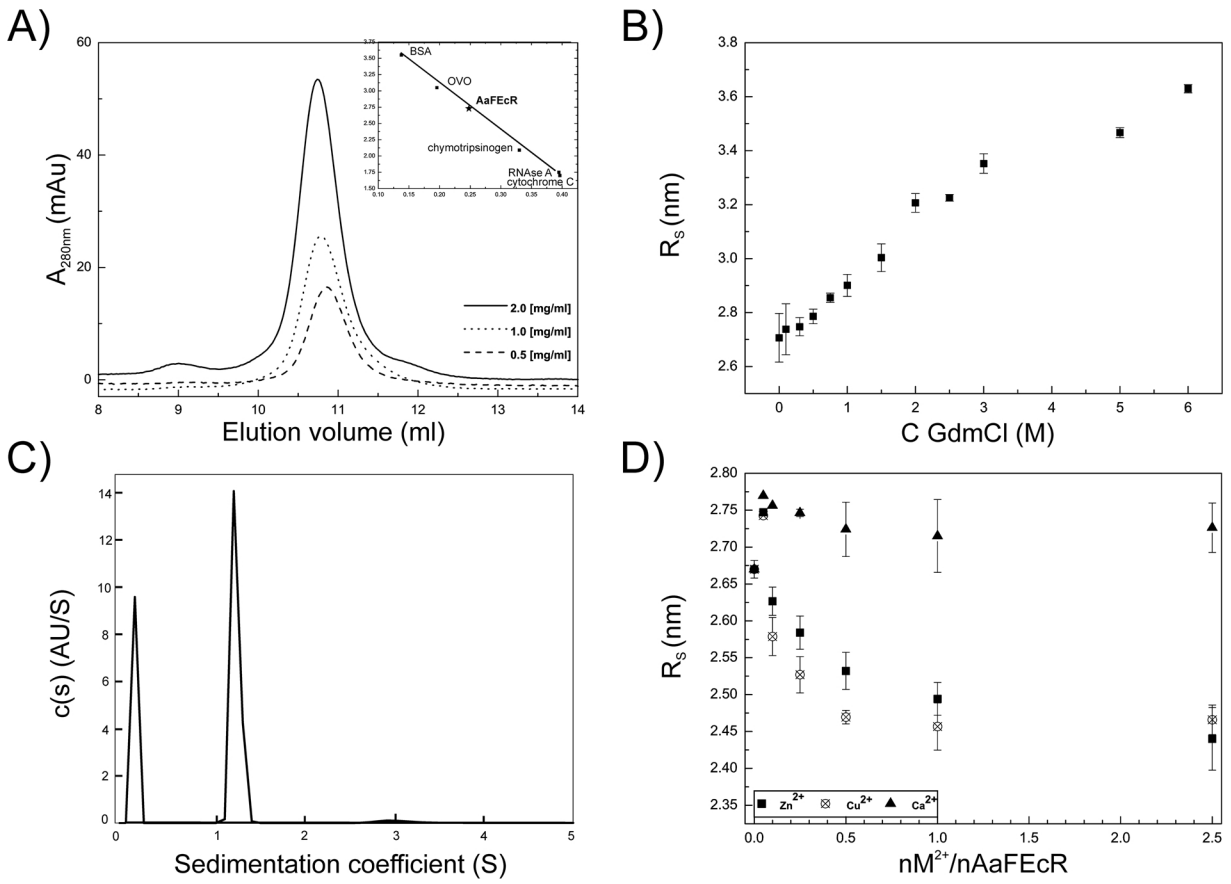

Fig. 4. Hydrodynamic properties of AaFEcR. A) Elution peaks of samples containing different AaFEcR concentrations. The inset shows the R_S values for standard proteins and AaFEcR plotted against their distribution coefficient (K_{av}). B) Change in the R_S of AaFEcR with increasing GdmCl concentrations examined with SEC. C) Normalized c(s) plotted against sedimentation coefficient [S] for native AaFEcR at the concentration of 0.5 mg/ml. D) Change in the R_S of AaFEcR determined using SEC in the presence of increasing Zn^{2+} (rectangle), Cu^{2+} (crossed circle) and Ca^{2+} (triangle) molar ratios. Experiments presented in A), B) and D) were performed in triplicate and the obtained results were averaged.

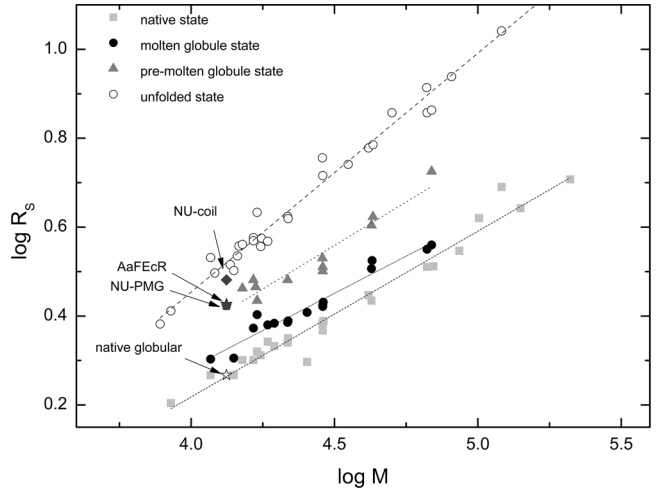

Fig. 5. AaFEcR behaves like natively unfolded pre-molten globules. The plot presents logarithmic values of R_S plotted against logarithmic values of molecular masses for proteins in native state (square), molten globule state (solid circle), pre-molten globule (triangle) and unfolded state (empty circle) [46,93]. AaFEcR was marked with the solid asterisk and AaFEcR considered as a theoretical native globular protein, NU-PMG or NU-coil was marked with empty asterisk, diamond and pentagon, respectively.

Table 1
Parameters derived from SV experiments.

c_{AaFEcR} [mg/ml]	s [S]	R_h [nm]	$R_{h,Svedberg}$ [nm]	f/f_0	MW_{app}	% of signal	RMSD
0.15	1.212	3.1	2.92	1.98	14128	96.0	0.004296
0.50	1.21	2.93	2.93	1.91	13309	98.3	0.005406
1.00	1.217	2.89	2.91	1.89	13207	95.2	0.006270

c_{AaFEcR} – concentration of AaFEcR, s – sedimentation coefficient, R_h – hydrodynamic radius, R_h/Svedberg – hydrodynamic radius calculated from the Svedberg equation, f/f0 – frictional ratio, MW_{app} – apparent molecular weight [g/mol], RMSD – root mean square deviation.

1346.9 $[Zn_2AaFEcRK]^{10+}$ increased (Suppl. Fig. 2). Equimolar Cu(II) complexes were detected at m/z = 1336.7 $[CuAaFEcR]^{10+}$ and 1340.5 $[CuAaFEcRK]^{10+}$. Even at this metal-to-ligand ratio, bimetallic species at m/z = 1342.8 $[Cu_2AaFEcR]^{10+}$ and traces of a $[Cu_3AaFEcR]^{10+}$ complex at m/z = 1349.0 were observed (Fig. 8). The intensity of signals corresponding to multimetal species, as well as the intensity of their potassium adducts at m/z 1346.6 $[Cu_2AaFEcRK]^{10+}$ and 1352.9 $[Cu_3AaFEcRK]^{10+}$, increased when a 2:1 Cu(II) to ligand ratio was used (Suppl. Fig. 3). AaFEcR seemed to bind fewer Ca^{2+} ions than Zn^{2+} and Cu^{2+} ions at each metal-to-ligand ratio. Only monomeric complexes were observed in both the 1:1 and 2:1 Ca(II) to ligand solutions (Fig. 9 and Suppl. Fig. 4, respectively). The intensity of the signals that correspond to the $[CaAaFEcRNa]^{10+}$ complex at m/z = 1336.5 and the $[CaAaFEcRNa_2K]^{10+}$ complex at m/z = 1342.8 increased when an additional Ca^{2+} equivalent was added. No traces of bimetallic complexes

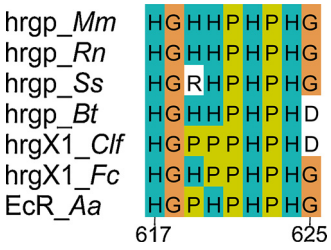

Fig. 6. AaFEcR possesses characteristic His-Pro-rich-like region of HPRGs. HPRG amino acid sequence fragments and a putative Zn^{2+}- and Cu^{2+}-binding motif from the F domain of the EcR from *Aedes aegypti* were compared in ClustalΩ [94] and imagined in Jalview [95]. Sequences were taken from the NCBI Server (https://www.ncbi.nlm.nih.gov/). The reference sequence numbers are as follows: *Mus musculus* (NP_444406.2), *Rattus norvegicus* (NP_596919.1), *Sus scrofa* (NP_001231568.1), *Bos taurus* (NP_776344.1), *Canis lupus familiaris* (XP_005639866.1), *Felis catus* (XP_003991881.1) and *Aedes aegypti* (AAA87394.1). Sequence numbering is relative to the amino acid residues in full-length EcR from *Aedes aegypti* (AAA87394.1) [10].

were observed under the studied conditions. The experimental isotopic patterns of the discussed complexes are in perfect agreement with the simulated ones (Fig. 7B and C, Suppl. Fig. 2B, Fig. 8B and C, Suppl. Fig. 3B and C, Fig. 9B and C and Suppl. Fig. 4B). Signals other than the mentioned ones correspond to potassium, sodium and perchlorate adducts of the free ligand and its metal complexes. The mass spectrometric observations are in excellent agreement with the dependencies observed in Fig. 4D, which shows that the R_S of the protein decreased upon the addition of Zn^{2+} and Cu^{2+}, while no pronounced changes were observed in the presence of Ca^{2+}. MS shows that AaFEcR is able to bind two Zn^{2+} and Cu^{2+} ions and only one Ca^{2+} ion when the metal-to-ligand ratio = 2:1. The observed difference in metal binding can be explained by their appropriate donor atom preferences and their preferred complex geometries. Usually, Zn^{2+} and Cu^{2+} ions have a high affinity for so-called intermediate metal-binding groups – most likely histidine imidazoles [50], and Cu^{2+} most likely also has affinity for amide nitrogens. Zn^{2+} prefers tetrahedral geometries, while Cu^{2+} favors octahedral or square planar and axially distorted octahedral geometries due to Jahn-Teller distortions of its d^9 electron configuration [51]. Ca^{2+}, on the other hand, is a so-called hard metal, with a high affinity for high hard metal-binding groups, e.g., carboxylic or carbonyl groups [52]; Ca^{2+} has a tendency to form octahedral complexes; and, Ca^{2+} binding is far more labile than Cu^{2+} or Zn^{2+} binding [53]. The stable binding of Cu^{2+} or Zn^{2+} metal ions causes AaFEcR to become more compact, most likely via the involvement of multiple histidine residues, which contributes to a distinct change in structure.

4. Discussion

Essential biological processes, including reproduction, development, homeostasis maintaining and metamorphosis, can be regulated by NRs. NRs are a superfamily of ligand-activated transcription factors [3]. Members of the NR superfamily share a common modular structure that generally consists of a C-terminal LBD linked by a flexible hinge region to the DBD, which is then flanked by an NTD that is hypervariable in sequence and length [1]. Many characterized proteins possess IDRs in their structures [20]. The lack of the 3D structure and existing as a set of conformers makes IDRs a challenge to study and identify [36]. IDPs play an important role in cellular regulation, signaling and control in health and disease. IDRs can perform various biological functions in proteins, such as DNA binding, protein-protein interactions, signal transduction and protein-macromolecular ligand or protein-metal ion interactions [54–59]. The level of structural disorder in proteins is thought to correlate with the number of interacting partners as a lack of folded structure might enable binding to multiple partners [60]. Moreover, the dimerization properties of IDPs or IDRs play an important role in their functions [27,61]. NRs possess variable IDRs, which are flexible linkers connecting globular domains, such as DBDs and LBDs, and flanking them at the N- and C-terminus, respectively. The structural-functional importance of IDRs in NRs is of great interest to scientists. The most characterized IDRs of NRs are their NTDs. It has been demonstrated that the NTDs of some NRs exhibit characteristics of IDRs and that these NTDs are unstructured in solution [27,62–66]. At the C-terminus of the LBDs of some NRs, there is also an additional region called the F domain that is defined as the amino acid residues after helix 12 of the LBDs. The F domain of NRs is the least conserved region in terms of length and sequence in the architecture of NRs (Fig. 10). The functional importance of the F domains of those NRs that possess them has not been extensively studied. However, it was suggested that the residual F domains of mammalian NRs might be involved in modulating NR activities by affecting transcriptional activation, dimerization, interactions with other proteins and/or stabilization of ligand binding by LBDs [23]. As mentioned above, the structure-function relationship of the F domains of the arthropod members of the NR superfamily remains unclear and enigmatic.

The unusual molecular properties observed for AaFEcR during its overexpression and successful purification led us to suppose that AaFEcR may be structurally disordered. To investigate whether AaFEcR belongs to the family of IDPs, a combination of diverse *in silico* analyses and wet-lab experiments was used. The CD spectra deconvolution reported approximately 30% ordered secondary structure (α-helix, β-sheet) and over 55% unordered regions in AaFEcR. The presence of residual ordered secondary structure in AaFEcR was also confirmed by SEC and CD in the presence of GdmCl. The structure-forming propensity of AaFEcR was induced by TFE and observed as the coil to helix transitions. Existing of AaFEcR as an IDR in EcR may take a part in ligand binding, posttranslational modifications, or interactions with appropriate partners. It cannot be ruled out that using this structural disorder and flexibility, AaFEcR may play a ligand-selective role for the LBD and through this function, modulate EcR activities via, for example, post-translational modifications. IDPs likely undergo posttranslational modifications in order to change their conformational state and/or perform functions [54]. The enrichment of serine residues in AaFEcR may not be accidental. The prediction with NetPhos 2.0 Server [67] (data not shown) indicated that 18 of 32 serine residues may undergo phosphorylation; thus, the function of this domain can be modulated. For instance, phosphorylation in the F domain of human estrogen receptor α (ERα) had a negative impact on transcriptional activity [68]; therefore, the impact of the potential phosphorylation of AaFEcR surely needs further research.

The DBD of NRs is the most conserved domain of NRs. The characteristic feature of the DBD in particular is two highly conserved zinc-finger motifs (C2C2), in which a Zn^{2+} is tetrahedrally coordinated by four highly evolutionally conserved cysteine residues [1,69]. In contrast to NRs, the classical C2H2 zinc-fingers possess two conserved cysteines and two conserved histidine residues [70]. However, other combinations of Cys/His as the zinc-chelating residues are possible too [71]. Our data showed that in addition to the DBD, another NR domain is able to bind metal ions. The HPRGs are involved in a number of processes, including blood coagulation, fibrinolysis, the immune response, and the transport of metal ions [72]. It was shown that the HPRG from rabbit serum binds Hg^{2+}, Cu^{2+}, Zn^{2+}, Ni^{2+}, Cd^{2+}, and Co^{2+} in descending order of binding affinity [73,74]. Metalloproteins, including HPRGs, containing metal ions coordinated by nitrogen, oxygen, or sulfur centers with different residues can be involved in a wide range of important biological processes, such as enzyme catalysis, signal transduction, transport, structure stabilization and storage [75–78]. The imidazole of histidine residues is a well-known coordinating ligand involved in enzyme-catalyzed reactions [79]; thus, the high content of histidine residues in AaFEcR may be related to its function involving the interaction with Zn^{2+} and Cu^{2+} ions. In cases of Zn^{2+} transporters, prion proteins, snake venoms, antimicrobial peptides and transcription

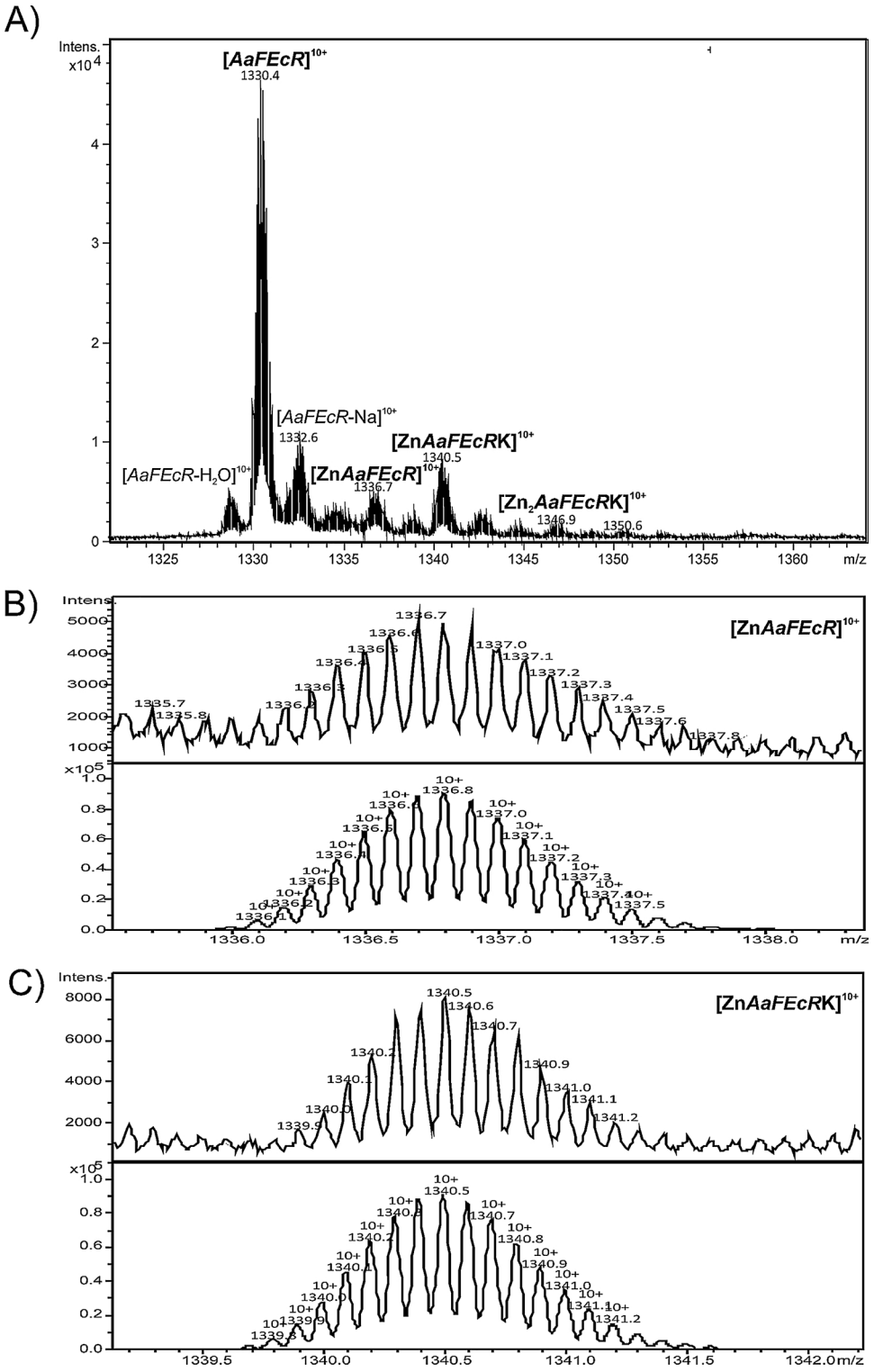

Fig. 7. Complexes of Zn^{2+}-AaFEcR. (A) The region z = 10+ of ESI-TOF MS spectrum for Zn^{2+}/AaFEcR = 1 was expanded for simplicity. The chosen signals are enlarged (B, C), and their experimental isotopic distributions (upper panels) are compared with the simulated ones (lower panels). Experiment was performed in triplicate.

factors, the coordination of metal ions is crucial for either the structure or function of the protein [80]. Moreover, Zn^{2+} and Cu^{2+} are important cofactors in the protective action of superoxide dismutase against oxidative damage [81]. Interestingly, it was shown that the antioxidant enzyme Cu/Zn superoxide dismutase (SOD1) can interact with ERα and enhance its DNA-binding activity [82]. To investigate in detail whether AaFEcR is capable of binding Zn^{2+} and Cu^{2+}, we conducted appropriate experiments using CD, SEC and MS techniques. The results clearly showed that recombinant AaFEcR is able to form complexes with Zn^{2+} and Cu^{2+}, but the interactions result in the protein shrinking rather than structuring. What is the functional importance of our present findings? Keeping in mind that the relation between metal ion binding, structure and function is one of the fundamental pillars of biology, we may hypothesize that the AaFEcR

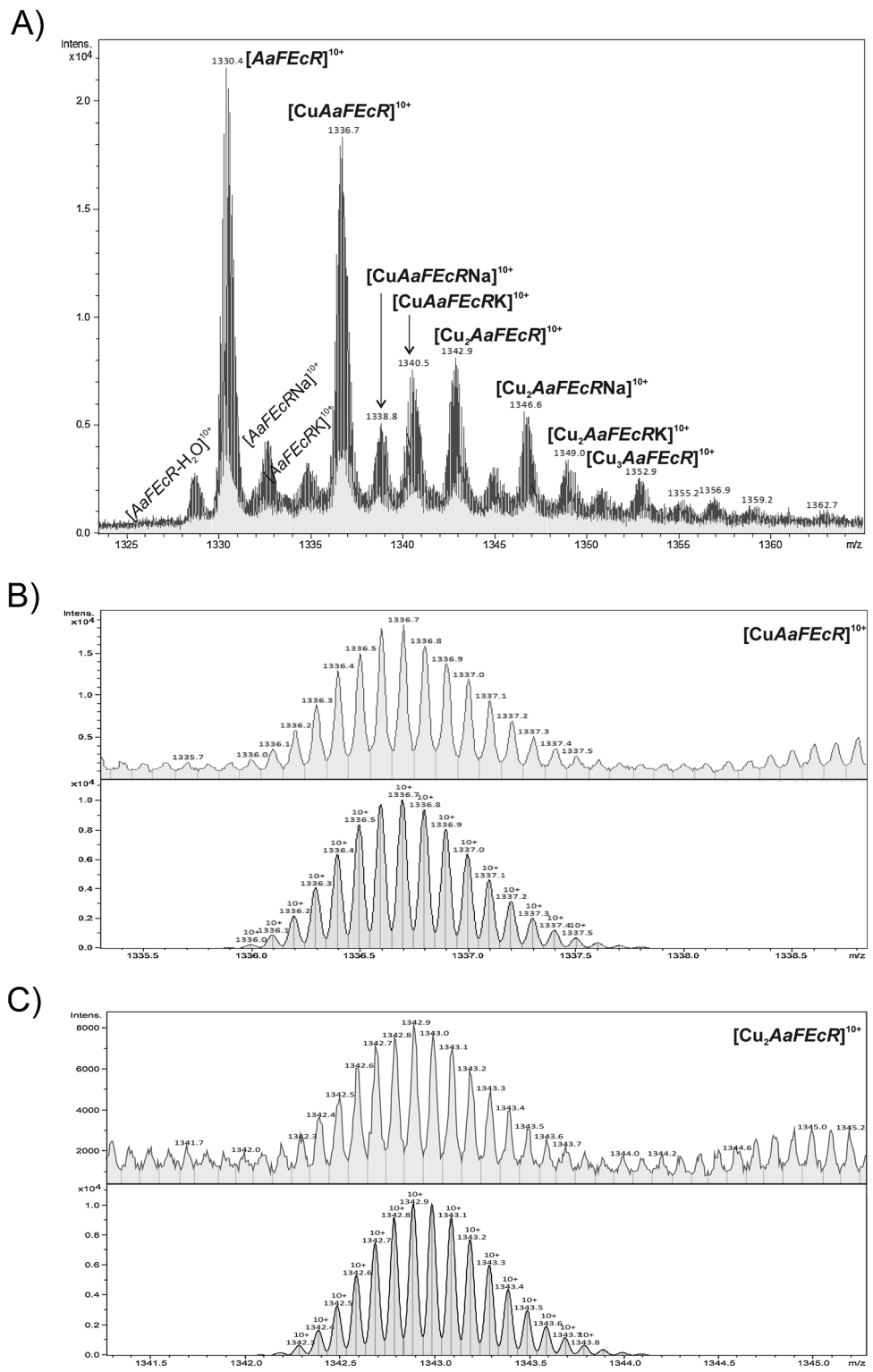

Fig. 8. Complexes of Cu^{2+}-AaFEcR. (A) The region z = 10+ of ESI-TOF MS spectrum for Cu^{2+}/AaFEcR = 1 was expanded for simplicity. The chosen signals are enlarged (B, C), and their experimental isotopic distributions (upper panels) are compared with the simulated ones (lower panels). Experiment was performed in triplicate.

compaction could lead to pronounced changes in the specificity and/or affinity of the interaction of the AaEcR with DNA or appropriate ligands or partners. The F domain of the EcR may function as a specific sensor of the respective ions to select the binding ligand or partner for the LBD, which may be important in modulating the EcR activities affecting the gene expression profiles of *A. aegypti*.

The EcR is a receptor of steroid hormones. In the case of mammalian NRs of steroid hormones, it was shown that metalloestrogens can modulate the function of estrogen receptor [83,84]. One of the vitellogenesis products, vitellogenin (Vg), is expressed in extra ovarian tissues in a specific manner upon blood meal, which is required to activate gene expression [17,19,85]. Analogous to the vertebrate liver, fat body, in insect females together with adipose tissue and lymph nodes is engaged in the production of yolk protein precursors (YPP) for

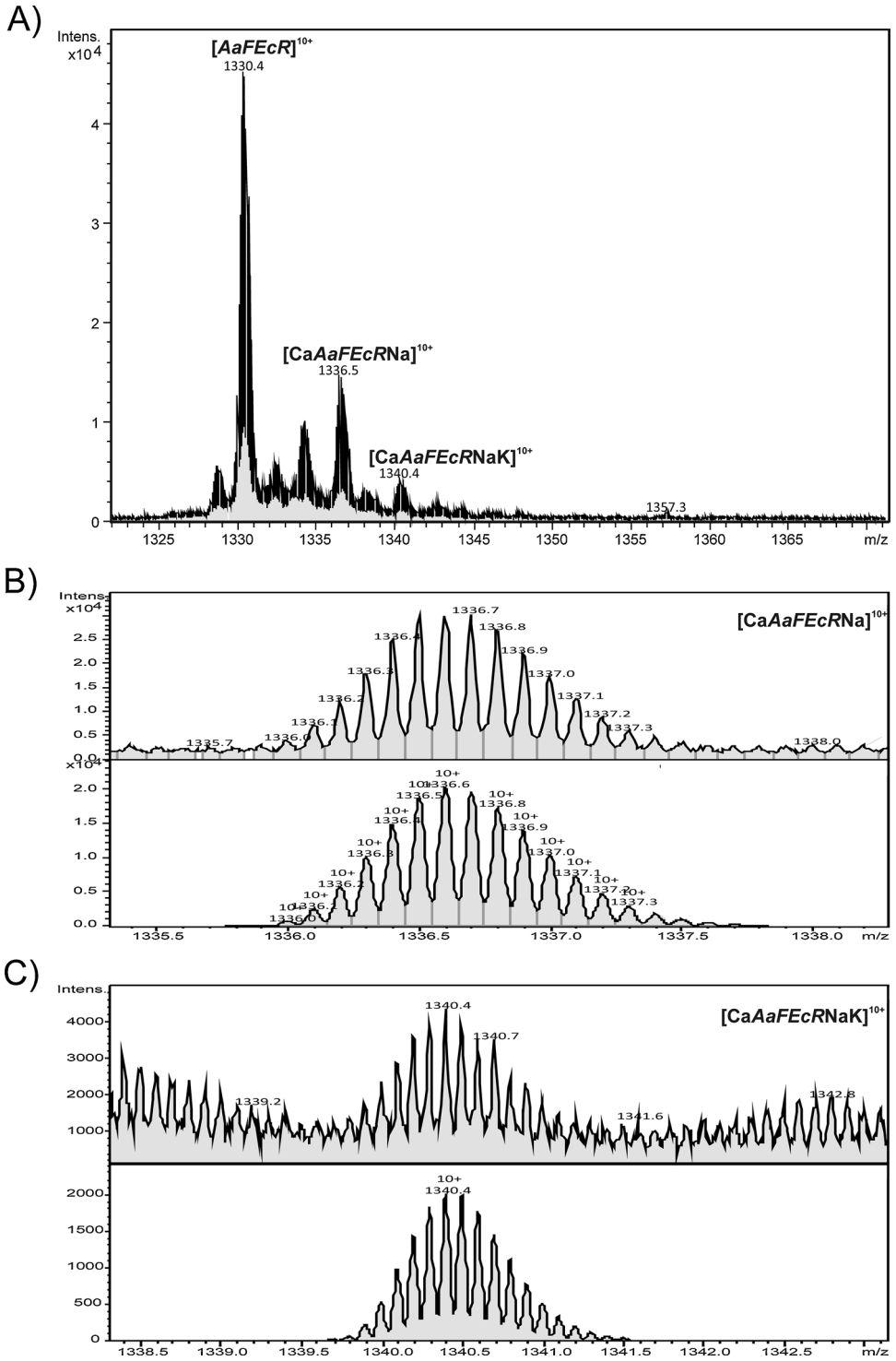

Fig. 9. Complexes of Ca^{2+}-AaFEcR. (A) The region z = 10+ of ESI-TOF MS spectrum for Ca^{2+}/AaFEcR = 1 was expanded for simplicity. The chosen signals are enlarged (B, C), and their experimental isotopic distributions (upper panels) are compared with the simulated ones (lower panels). Experiment was performed in triplicate.

developing oocytes [17]. A blood meal triggers a 20E cascade that activates YPP genes in the *A. aegypti* fat body [19,86]. It was shown that the *A. aegypti* EcR/Usp heterodimer directly binds the Vg gene promoter [24]. Interestingly, it was shown that Vg may act as a Zn^{2+} carrier that protects honeybee workers and queens from oxidative stress [87–89]. The blood meal itself leads to metabolic changes and induces a state of oxidative stress [90]. Therefore, it is possible that the expression of the Vg gene may depend on Zn^{2+} concentration changes sensed by AaFEcR in the EcR/Usp heterodimer. Moreover, it was suggested that antioxidant defense is one of the mechanisms by which mosquito cells survive dengue 2 viral infection [91]. Detoxification enzymes may play an important role in modulating host immunity [92]. Thus, a functional EcR may modulate the metal-responsive transcriptional regulation of the expression of genes encoding oxidative stress-protective proteins. However, the physiological role of ion metal binding by AaFEcR in the context of the full-length EcR activities in *A. aegypti* is still unknown.

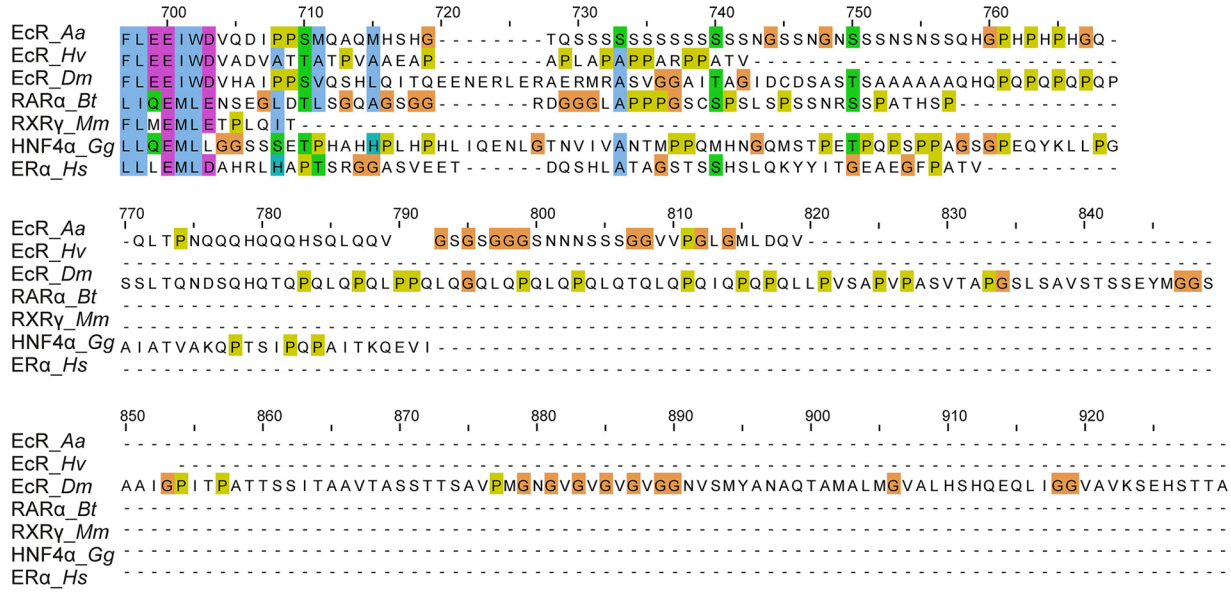

Fig. 10. C-terminal domains from various nuclear receptors are not conserved in sequence and length. NR amino acid sequences were compared in ClustalΩ [94] and imagined in Jalview [95]. Sequences were taken from the NCBI Server (https://www.ncbi.nlm.nih.gov/). The abbreviations and reference sequence numbers are as follows: EcR from *A. aegypti* - EcR_*Aa* (AAA87394.1), EcR from *H. virescens* - EcR_*Hv* (CAA70212.1), ecdysone receptor, isoform A from *D. melanogaster* - EcR_*Dm* (NP_724456.1), retinoic acid receptor α from *B. taurus* - RARα_*Bt* (NP_001014942.2), retinoid X receptor γ from *M. musculus* - RXRγ_*Mm* (EDL39178.1), hepatocyte nuclear factor 4 α from *G. gallus* - HNF4α_*Gg* (NP_001026026.1) and estrogen nuclear receptor α from *H. sapiens* - ERα_*Hs* (AEP43755.1). Sequence numbering is relative to the longest sequence belonging to *D. melanogaster* - EcR_*Dm* (NP_724456.1).

Acknowledgments

This study was supported by a statutory activity subsidy from the Polish Ministry of Science and Higher Education for the Faculty of Chemistry of Wrocław University of Science and Technology and from the National Science Centre (no. UMO-2014/13/D/ST5/02868). The publication costs were provided by the Wrocław Centre of Biotechnology Programme: Leading National Research Centre (KNOW) from 2014–2018. We are grateful to Mirosława Ostrowska, Eng. (Wrocław University of Science and Technology) for her excellent technical assistance and to Natalia Bagińska, M.Sc. Eng. (Wrocław University of Science and Technology) for her assistance during initial protein purification. In addition, we are grateful to Professor Henryk Kozłowski (Faculty of Chemistry, University of Wrocław, Poland) for giving us the opportunity to perform protein-metal ESI-TOF MS experiments.

Appendix A. Supplementary data

Supplementary material related to this article can be found, in the online version, at doi: https://doi.org/10.1016/j.jsbmb.2018.09.008.

References

[1] M.M. Aagaard, R. Siersbæk, S. Mandrup, Molecular basis for gene-specific transactivation by nuclear receptors, Biochim. Biophys. Acta - Mol. Basis Dis. 1812 (2011) 824–835, https://doi.org/10.1016/j.bbadis.2010.12.018.
[2] L. Altucci, H. Gronemeyer, Nuclear receptors in cell life and death, Trends Endocrinol. Metab. 12 (2001) 460–468, https://doi.org/10.1016/S1043-2760(01)00502-1.
[3] A. Aranda, A. Pascual, Nuclear hormone receptors and gene expression, Physiol. Rev. 81 (2001) 1269–1304 http://www.ncbi.nlm.nih.gov/pubmed/11427696.
[4] D. Gkikas, M. Tsampoula, P.K. Politis, Nuclear receptors in neural stem/progenitor cell homeostasis, Cell. Mol. Life Sci. 74 (2017) 4097–4120, https://doi.org/10.1007/s00018-017-2571-4.
[5] I.J. Mcewan, R. Kumar, Nuclear Receptors: From Structure to the Clinic, (2015), pp. 1–14, https://doi.org/10.1007/978-3-319-18729-7.
[6] L.M. Riddiford, J.W. Truman, Hormone receptors and the regulation of insect metamorphosis, Integr. Comp. Biol. 33 (1993) 340–347, https://doi.org/10.1093/icb/33.3.340.
[7] K.D. Spindler, C. Hönl, C. Tremmel, S. Braun, H. Ruff, M. Spindler-Barth, Ecdysteroid hormone action, Cell. Mol. Life Sci. 66 (2009) 3837–3850, https://doi.org/10.1007/s00018-009-0112-5.
[8] A.S. Raikhel, K. Miura, W.A. Segraves, Nuclear receptors in mosquito vitellogenesis, Integr. Comp. Biol. 39 (1999) 722–735, https://doi.org/10.1093/icb/39.4.722.
[9] M.R. Koelle, W.S. Talbot, W.A. Segraves, M.T. Bender, P. Cherbas, D.S. Hogness, The Drosophila EcR gene encodes an ecdysone receptor, a new member of the steroid receptor superfamily, Cell 67 (1991) 59–77, https://doi.org/10.1016/0092-8674(91)90572-G.
[10] W.L. Cho, M.Z. Kapitskaya, A.S. Raikhel, Mosquito ecdysteroid receptor: analysis of the cDNA and expression during vitellogenesis, Insect Biochem. Mol. Biol. 25 (1995) 19–27, https://doi.org/10.1016/0965-1748(94)00045-J.
[11] T.P. Yao, W.A. Segraves, A.E. Oro, M. McKeown, R.M. Evans, Drosophila ultraspiracle modulates ecdysone receptor function via heterodimer formation, Cell 71 (1992) 63–72, https://doi.org/10.1016/0092-8674(92)90266-F.
[12] M. Kapitskaya, S. Wang, D.E. Cress, T.S. Dhadialla, A.S. Raikhel, The mosquito ultraspiracle homologue, a partner of ecdysteroid receptor heterodimer: cloning and characterization of isoforms expressed during vitellogenesis, Mol. Cell. Endocrinol. 121 (1996) 119–132, https://doi.org/10.1016/0303-7207(96)03847-6.
[13] M.G. Guzman, S.B. Halstead, H. Artsob, P. Buchy, J. Farrar, M.B. Nathan, J.L. Pelegrino, C. Simmons, S. Yoksan, Dengue : a continuing global threat Europe PMC funders author manuscripts, Nat. Rev. Microbiol. 8 (2010) S7–S16, https://doi.org/10.1038/nrmicro2460.Dengue.
[14] A.D.T. Barrett, S. Higgs, Yellow fever: a disease that has yet to be conquered, Annu. Rev. Entomol. 52 (2007) 209–229, https://doi.org/10.1146/annurev.ento.52.110405.091454.
[15] N.J. Marchette, R. Garcia, A. Rudnick, Isolation of Zika virus from Aedes aegypti mosquitoes in Malaysia, Am. J. Trop. Med. Hyg. 18 (1969) 411–415 http://www.ncbi.nlm.nih.gov/pubmed/4976739.
[16] K.A. Tsetsarkin, R. Chen, S.C. Weaver, Interspecies transmission and chikungunya virus emergence, Curr. Opin. Virol. 16 (2016) 143–150, https://doi.org/10.1016/j.coviro.2016.02.007.
[17] A.S. Raikhel, T.S. Dhadialla, Accumulation of yolk proteins in insect oocytes, Annu. Rev. Entomol. 37 (1992) 217–251, https://doi.org/10.1146/annurev.ento.37.1.217.
[18] G.M. Attardo, I.A. Hansen, A.S. Raikhel, Nutritional regulation of vitellogenesis in mosquitoes: implications for anautogeny, Insect Biochem. Mol. Biol. 35 (2005) 661–675, https://doi.org/10.1016/j.ibmb.2005.02.013.
[19] A.S. Raikhel, V. Kokoza, J. Zhu, D. Martin, S.F. Wang, C. Li, G. Sun, A. Ahmed, N. Dittmer, G. Attardo, Molecular biology of mosquito vitellogenesis: from basic studies to genetic engineering of antipathogen immunity, Insect Biochem. Mol. Biol. 32 (2002) 1275–1286, https://doi.org/10.1016/S0965-1748(02)00090-5.
[20] V.N. Uversky, Unusual biophysics of intrinsically disordered proteins, Biochim. Biophys. Acta - Proteins Proteom. 1834 (2013) 932–951, https://doi.org/10.1016/j.bbapap.2012.12.008.
[21] M. Wojtas, R. Hołubowicz, M. Poznar, M. Maciejewska, A. Ożyhar, P. Dobryszycki, Calcium ion binding properties and the effect of phosphorylation on the intrinsically disordered starmaker protein, Biochemistry 54 (2015) 6525–6534, https://doi.org/10.1021/acs.biochem.5b00933.

[22] P. Faller, C. Hureau, G. La Penna, Metal ions and intrinsically disordered proteins and peptides: from Cu/Zn amyloid-β to general principles, Acc. Chem. Res. 47 (2014) 2252–2259, https://doi.org/10.1021/ar400293h.
[23] S.R. Patel, D.F. Skafar, Modulation of nuclear receptor activity by the F domain, Mol. Cell. Endocrinol. 418 (2015) 298–305, https://doi.org/10.1016/j.mce.2015.07.009.
[24] D. Martín, S.F. Wang, A.S. Raikhel, The vitellogenin gene of the mosquito Aedes aegypti is a direct target of ecdysteroid receptor, Mol. Cell. Endocrinol. 173 (2001) 75–86, https://doi.org/10.1016/S0303-7207(00)00413-5.
[25] U.K. Laemmli, Cleavage of structural proteins during the assembly of the head of bacteriophage T4, Nature 227 (5259) (1970) 680–685.
[26] G. Fairbanks, T.L. Steck, D. Wallach, Electrophoretic analysis of the major polypeptides of the human erythrocyte membrane, Biochemistry 10 (1971) 2606–2617.
[27] J. Pieprzyk, A. Zbela, M. Jakób, A. Ozyhar, M. Orłowski, Homodimerization propensity of the intrinsically disordered N-terminal domain of ultraspiracle from Aedes aegypti, Biochim. Biophys. Acta - Proteins Proteom. 1844 (2014) 1153–1166, https://doi.org/10.1016/j.bbapap.2014.03.010.
[28] Z. Dosztanyi, V. Csizmok, P. Tompa, I. Simon, IUPred: web server for the prediction of intrinsically unstructured regions of proteins based on estimated energy content, Bioinformatics 21 (2005) 3433–3434, https://doi.org/10.1093/bioinformatics/bti541.
[29] P. Romero, Z. Obradovic, X. Li, E.C. Garner, C.J. Brown, A.K. Dunker, Sequence complexity of disordered protein, Proteins 42 (2001) 38–48 http://www.ncbi.nlm.nih.gov/pubmed/11093259.
[30] K. Peng, S. Vucetic, P. Radivojac, C.J. Brown, A.K. Dunker, Z. Obradovic, Optimizing long intrinsic disorder predictors with protein evolutionary information, J. Bioinform. Comput. Biol. 3 (2005) 35–60 http://www.ncbi.nlm.nih.gov/pubmed/15751111.
[31] K. Peng, P. Radivojac, S. Vucetic, A.K. Dunker, Z. Obradovic, Length-dependent prediction of protein intrinsic disorder, BMC Bioinf. 7 (2006) 208, https://doi.org/10.1186/1471-2105-7-208.
[32] B. Xue, R.L. Dunbrack, R.W. Williams, A.K. Dunker, V.N. Uversky, PONDR-FIT: a meta-predictor of intrinsically disordered amino acids, Biochim. Biophys. Acta - Proteins Proteom. 1804 (2010) 996–1010, https://doi.org/10.1016/j.bbapap.2010.01.011.
[33] D.T. Jones, J.J. Ward, Prediction of disordered regions in proteins from position specific score matrices, Proteins Struct. Funct. Genet. 53 (2003) 573–578, https://doi.org/10.1002/prot.10528.
[34] V. Vacic, V.N. Uversky, A.K. Dunker, S. Lonardi, Composition profiler: a tool for discovery and visualization of amino acid composition differences, BMC Bioinf. 8 (2007) 211, https://doi.org/10.1186/1471-2105-8-211.
[35] J. Prilusky, C.E. Felder, T. Zeev-Ben-Mordehai, E.H. Rydberg, O. Man, J.S. Beckmann, I. Silman, J.L. Sussman, FoldIndex: a simple tool to predict whether a given protein sequence is intrinsically unfolded, Bioinformatics 21 (2005) 3435–3438, https://doi.org/10.1093/bioinformatics/bti537.
[36] V.N. Uversky, J.R. Gillespie, A.L. Fink, Why are "natively unfolded" proteins unstructured under physiologic conditions? Proteins 41 (2000) 415–427, https://doi.org/10.1002/1097-0134(20001115)41.
[37] P. Andrews, Estimation of molecular size and molecular weights of biological compounds by gel filtration, Methods Biochem. Anal. 18 (1970) 1–53.
[38] A. Savitzky, M.J.E. Golay, Smoothing and differentiation of data by simplified least squares procedures, Anal. Chem. 36 (1964) 1627–1639, https://doi.org/10.1021/ac60214a047.
[39] S.M. Kelly, T.J. Jess, N.C. Price, How to study proteins by circular dichroism, Biochim. Biophys. Acta - Proteins Proteom. 1751 (2005) 119–139, https://doi.org/10.1016/j.bbapap.2005.06.005.
[40] N. Sreerama, R.W. Woody, Estimation of protein secondary structure from circular dichroism spectra: comparison of CONTIN, SELCON, and CDSSTR methods with an expanded reference set, Anal. Biochem. 287 (2000) 252–260, https://doi.org/10.1006/abio.2000.4880.
[41] M.L. Tiffany, S. Krimm, Extended conformations of polypeptides and proteins in urea and guanidine hydrochloride, Biopolymers 12 (1973) 575–587, https://doi.org/10.1002/bip.1973.360120310.
[42] H. Zhao, R. Ghirlando, G. Piszczek, U. Curth, C.A. Brautigam, P. Schuck, Recorded scan times can limit the accuracy of sedimentation coefficients in analytical ultracentrifugation, Anal. Biochem. 437 (2013) 104–108, https://doi.org/10.1016/j.ab.2013.02.011.
[43] P. Schuck, Size-Distribution Analysis of Macromolecules by Sedimentation Velocity Ultracentrifugation and Lamm Equation Modeling 78 (2000), pp. 1606–1619.
[44] V.N. Uversky, Natively unfolded proteins: a point where biology waits for physics, Protein Sci. 11 (2002) 739–756, https://doi.org/10.1110/ps.4210102.
[45] R.W. Woody, Circular dichrosim of intrinsically disordered proteins, Instrum. Anal. Intrinsically Disord. Proteins Assess. Struct. Conform. (2010) 303–321.
[46] V.N. Uversky, What does it mean to be natively unfolded? Eur. J. Biochem. 269 (2002) 2–12, https://doi.org/10.1110/ps.4210102.matic.
[47] M. Poznar, R. Hołubowicz, M. Wojtas, J. Gapiński, E. Banachowicz, A. Patkowski, A. Ożyhar, P. Dobryszycki, Structural properties of the intrinsically disordered, multiple calcium ion-binding otolith matrix macromolecule-64 (OMM-64), Biochim. Biophys. Acta - Proteins Proteom. 1865 (2017) 1358–1371, https://doi.org/10.1016/j.bbapap.2017.08.019.
[48] F. Manon, C. Ebel, Analytical ultracentrifugation, a useful tool to probe intrinsically disordered proteins, Instrum. Anal. Intrinsically Disord. Proteins, John Wiley & Sons, Inc., Hoboken, NJ, USA, 2010, pp. 431–449, https://doi.org/10.1002/9780470602614 ch15..
[49] M. Ranieri-Raggi, A. Moir, A. Raggi, The role of histidine-proline-Rich glycoprotein as zinc chaperone for skeletal muscle AMP deaminase, Biomolecules 4 (2014) 474–497, https://doi.org/10.3390/biom4020474.
[50] S. Rajković, C. Kállay, R. Serényi, G. Malandrinos, N. Hadjiliadis, D. Sanna, I. Sóvágó, Complex formation processes of terminally protected peptides containing two or three histidyl residues. Characterization of the mixed metal complexes of peptides, Dalton Trans. (2008) 5059–5071, https://doi.org/10.1039/b808323a.
[51] K.L. Haas, K.J. Franz, NIH Public Access vol. 109, (2010), pp. 4921–4960, https://doi.org/10.1021/cr900134a.Application.
[52] T. Bala, B.L.V. Prasad, M. Sastry, M.U. Kahaly, U.V. Waghmare, Interaction of different metal ions with carboxylic acid group: a quantitative study, J. Phys. Chem. A 111 (2007) 6183–6190, https://doi.org/10.1021/jp067906x.
[53] A.K. Katz, J.P. Glusker, S.A. Beebe, C.W. Bock, Calcium ion coordination: a comparison with that of beryllium, magnesium, and zinc, J. Am. Chem. Soc. 118 (1996) 5752–5763, https://doi.org/10.1021/ja953943i.
[54] R. Van Der Lee, M. Buljan, B. Lang, R.J. Weatheritt, G.W. Daughdrill, A.K. Dunker, M. Fuxreiter, J. Gough, J. Gsponer, D.T. Jones, P.M. Kim, R.W. Kriwacki, C.J. Oldfield, R.V. Pappu, P. Tompa, V.N. Uversky, P.E. Wright, M.M. Babu, Classification of intrinsically disordered regions and proteins, Chem. Rev. 114 (2014) 6589–6631, https://doi.org/10.1021/cr400525m.
[55] A.K. Dunker, S.E. Bondos, F. Huang, C.J. Oldfield, Intrinsically disordered proteins and multicellular organisms, Semin. Cell Dev. Biol. 37 (2015) 44–55, https://doi.org/10.1016/j.semcdb.2014.09.025.
[56] K. Dunker, C. Brown, D. Lawson, L. Iakoucheva, Z. Obradovic, Current topics intrinsic disorder and protein function †, Proteins 41 (2002).
[57] M. Krasowski, E. Reschly, Intrinsic disorder in nuclear hormone receptors, J. Proteome. 7 (2008) 4359–4372, https://doi.org/10.1021/pr8003024.INTRINSIC.
[58] J. Liu, N.B. Perumal, C.J. Oldfield, E.W. Su, V.N. Uversky, A.K. Dunker, Intrinsic disorder in transcription factors, Biochemistry 45 (2006) 6873–6888, https://doi.org/10.1021/bi0602718.
[59] P.E. Wright, H.J. Dyson, Intrinsically disordered proteins in cellular signaling and regulation, Nat. Rev. Mol. Cell Biol. 16 (2015) 18–29, https://doi.org/10.1038/nrm3920.Intrinsically.
[60] L.M. Iakoucheva, C.J. Brown, J.D. Lawson, Z. Obradović, A.K. Dunker, Intrinsic disorder in cell-signaling and cancer-associated proteins, J. Mol. Biol. 323 (2002) 573–584, https://doi.org/10.1016/S0022-2836(02)00969-5.
[61] A.B. Sigalov, Structural biology of intrinsically disordered proteins: revisiting unsolved mysteries, Biochimie 125 (2016) 112–118, https://doi.org/10.1016/j.biochi.2016.03.006.
[62] A. Wärnmark, A. Wikström, A.P.H. Wright, J.Å. Gustafsson, T. Härd, The N-terminal regions of estrogen receptor α and β are unstructured in vitro and show different TBP binding properties, J. Biol. Chem. 276 (2001) 45939–45944, https://doi.org/10.1074/jbc.M107875200.
[63] J. Reid, S.M. Kelly, K. Watt, N.C. Price, I.J. McEwan, Conformational analysis of the androgen receptor amino-terminal domain involved in transactivation. Influence of structure-stabilizing solutes and protein-protein interactions, J. Biol. Chem. 277 (2002) 20079–20086, https://doi.org/10.1074/jbc.M201003200.
[64] M. Nocula-Ługowska, G. Rymarczyk, M. Lisowski, A. Ozyhar, Isoform-specific variation in the intrinsic disorder of the ecdysteroid receptor N-terminal domain, Proteins Struct. Funct. Bioinf. 76 (2009) 291–308, https://doi.org/10.1002/prot.22342.
[65] A. Dziedzic-Letka, G. Rymarczyk, T.M. Kapłon, A. Górecki, A. Szamborska-Gbur, M. Wojtas, P. Dobryszycki, A. Ozyhar, Intrinsic disorder of Drosophila melanogaster hormone receptor 38 N-terminal domain, Proteins Struct. Funct. Bioinf. 79 (2011) 376–392, https://doi.org/10.1002/prot.22887.
[66] A.Y. Belorusova, J. Osz, M.V. Petoukhov, C. Peluso-Iltis, B. Kieffer, D.I. Svergun, N. Rochel, Solution behavior of the intrinsically disordered N-Terminal domain of retinoid X receptor α in the context of the full-length protein, Biochemistry 55 (2016) 1741–1748, https://doi.org/10.1021/acs.biochem.5b01122.
[67] N. Blom, S. Gammeltoft, S. Brunak, Sequence and structure-based prediction of eukaryotic protein phosphorylation sites, J. Mol. Biol. 294 (1999) 1351–1362, https://doi.org/10.1006/jmbi.1999.3310.
[68] S. Marqusee, V.H. Robbins, R.L. Baldwin, Unusually stable helix formation in short alanine-based peptides, Proc. Natl. Acad. Sci. U. S. A. 86 (1989) 5286–5290, https://doi.org/10.1073/pnas.86.14.5286.
[69] J.P. Renaud, D. Moras, Structural studies on nuclear receptors, Cell. Mol. Life Sci. 57 (2000) 1748–1769.
[70] J.H. Laity, B.M. Lee, P.E. Wright, Zinc finger proteins: new insights into structural and functional diversity, Curr. Opin. Struct. Biol. 11 (2001) 39–46, https://doi.org/10.1016/S0959-440X(00)00167-6.
[71] S.S. Krishna, I. Majumdar, N.V. Grishin, Structural classification of zinc fingers, Nucleic Acids Res. 31 (2003) 532–550, https://doi.org/10.1093/nar/gkg161.
[72] C.B. Peterson, W.T. Morgan, M.N. Blackburn, Histidine-rich glycoprotein modulation of the anticoagulant activity of heparin. Evidence for a mechanism involving competition with both antithrombin and thrombin for heparin binding, J. Biol. Chem. 262 (1987) 7567–7574.
[73] W.T. Morgan, Interactions of the histidine-rich glycoprotein of serum with metals, Biochemistry 20 (1981) 1054–1061, https://doi.org/10.1021/bi00508a002.
[74] S.L. Guthans, W.T. Morgan, The interaction of zinc, nickel and cadmium with serum albumin and histidine-rich glycoprotein assessed by equilibrium dialysis and immunoadsorbent chromatography, Arch. Biochem. Biophys. 218 (1982) 320–328, https://doi.org/10.1016/0003-9861(82)90350-2.
[75] H. Feinberg, H.M. Greenblatt, G. Shoham, Structural studies of the role of the active site metal in Metalloenzymes, J. Chem. Inf. Comput. Sci. 33 (1993) 501–516, https://doi.org/10.1021/ci00013a030.
[76] J.P. Hosler, S. Ferguson-miller, D.A. Mills, NIH public access, Annu. Rev. Biochem. 75 (2006) 165–187, https://doi.org/10.1146/annurev.biochem.75.062003.101730.Energy.

[77] S. Mongkolsuk, J.D. Helmann, Regulation of inducible peroxide stress responses, Mol. Microbiol. 45 (2002) 9–15, https://doi.org/10.1046/j.1365-2958.2002.03015.x.
[78] J.S. Valentine, P.A. Doucette, S. Zittin Potter, Copper-zinc superoxide dismutase and amyotrophic lateral sclerosis, Annu. Rev. Biochem. 74 (2005) 563–593, https://doi.org/10.1146/annurev.biochem.72.121801.161647.
[79] S.M. Liao, Q.S. Du, J.Z. Meng, Z.W. Pang, R.B. Huang, The multiple roles of histidine in protein interactions, Chem. Cent. J. 7 (2013) 9–11, https://doi.org/10.1186/1752-153X-7-44.
[80] M. Rowinska-Zyrek, D. Witkowska, S. Potocki, M. Remelli, H. Kozlowski, His-rich sequences – is plagiarism from nature a good idea? New J. Chem. 37 (2013) 58–70, https://doi.org/10.1039/C2NJ40558J.
[81] T. Fukai, M. Ushio-Fukai, Superoxide dismutases: role in redox signaling, vascular function, and diseases, Antioxid. Redox Signal. 15 (2011) 1583–1606, https://doi.org/10.1089/ars.2011.3999.
[82] A.K. Rao, Y.S. Ziegler, I.X. McLeod, J.R. Yates, A.M. Nardulli, Effects of Cu/Zn superoxide dismutase on estrogen responsiveness and oxidative stress in human breast cancer cells, Mol. Endocrinol. 22 (2008) 1113–1124, https://doi.org/10.1210/me.2007-0381.
[83] C. Byrne, S.D. Divekar, G.B. Storchan, D.A. Parodi, M.B. Martin, Metals and breast Cancer, J. Mamm. Gland Biol. Neoplasia 18 (2013) 63–73, https://doi.org/10.1007/s10911-013-9273-9.
[84] P.D. Darbre, Aluminium, antiperspirants and breast cancer, J. Inorg. Biochem. 99 (2005) 1912–1919, https://doi.org/10.1016/j.jinorgbio.2005.06.001.
[85] I.A. Hansen, G.M. Attardo, S.D. Rodriguez, L.L. Drake, Four-way regulation of mosquito yolk protein precursor genes by juvenile hormone-, ecdysone-, nutrient-, and insulin-like peptide signaling pathways, Front. Physiol. 5 (2014) 1–8, https://doi.org/10.3389/fphys.2014.00103.
[86] W.C. Marquardt, Biology od Disease Vectors, Acad. Press. Inc., 2004.
[87] G.V. Amdam, Z.L.P. Simões, A. Hagen, K. Norberg, K. Schrøder, Ø. Mikkelsen, T.B.L. Kirkwood, S.W. Omholt, Hormonal control of the yolk precursor vitellogenin regulates immune function and longevity in honeybees, Exp. Gerontol. 39 (2004) 767–773, https://doi.org/10.1016/j.exger.2004.02.010.
[88] G.V. Amdam, K. Norberg, M.K. Fondrk, R.E. Page, Reproductive ground plan may mediate colony-level selection effects on individual foraging behavior in honey bees, Proc. Natl. Acad. Sci. 101 (2004) 11350–11355, https://doi.org/10.1073/pnas.0403073101.
[89] S.-C. Seehuus, K. Norberg, U. Gimsa, T. Krekling, G.V. Amdam, Reproductive protein protects functionally sterile honey bee workers from oxidative stress, Proc. Natl. Acad. Sci. 103 (2006) 962–967, https://doi.org/10.1073/pnas.0502681103.
[90] S. Kumar, L. Gupta, S.H. Yeon, C. Barillas-Mury, Inducible peroxidases mediate nitration of Anopheles midgut cells undergoing apoptosis in response to Plasmodium invasion, J. Biol. Chem. 279 (2004) 53475–53482, https://doi.org/10.1074/jbc.M409905200.
[91] T.H. Chen, P. Tang, C.F. Yang, L.H. Kao, Y.P. Lo, C.K. Chuang, Y.T. Shih, W.J. Chen, Antioxidant defense is one of the mechanisms by which mosquito cells survive dengue 2 viral infection, Virology 410 (2011) 410–417, https://doi.org/10.1016/j.virol.2010.12.013.
[92] R.K. Chaitanya, P. Sridevi, K.S. Kumar, B.S. Mastan, K.A. Kumar, A. Dutta-Gupta, Expression analysis of reactive oxygen species detoxifying enzyme genes in Anopheles stephensi during Plasmodium berghei midgut invasion, Asian Pac. J. Trop. Med. 7 (2014) 680–684, https://doi.org/10.1016/S1995-7645(14)60116-4.
[93] V.N. Uversky, Use of fast protein size-exclusion liquid chromatography to study the unfolding of proteins which denature through the molten globule, Biochemistry. 32 (1993) 13288–13298, https://doi.org/10.1021/bi00211a042.
[94] W. Li, A. Cowley, M. Uludag, T. Gur, H. McWilliam, S. Squizzato, Y.M. Park, N. Buso, R. Lopez, The EMBL-EBI bioinformatics web and programmatic tools framework, Nucleic Acids Res. 43 (2015) W580–W584, https://doi.org/10.1093/nar/gkv279.
[95] A.M. Waterhouse, J.B. Procter, D.M.A. Martin, M. Clamp, G.J. Barton, Jalview Version 2–a multiple sequence alignment editor and analysis workbench, Bioinformatics 25 (2009) 1189–1191, https://doi.org/10.1093/bioinformatics/btp033.